

OPTIMUM AND DESIGN TRENDS OF COMPOUND HELICOPTERS

Omri Rand, Vladimir Khromov
Faculty of Aerospace Engineering,
Technion - Israel Institute of Technology,
Haifa 3200003, Israel

Keywords: *Compound Helicopters, Lift Offset*

Abstract

The present paper is focused on the complex task of design and optimizing a compound helicopter configuration. The analysis is founded on the “Drag vs. Power Chart” methodology that enable the separation of the rotors, thrusters, wings and fuselage contributions and understanding their optimal combination in a generic compound configuration. The paper also supplies an optimization process which is based on a comprehensive and detailed nonlinear free-wake analysis of a compound configuration that includes a thruster and fixed wings. The configurations on the resulting Pareto frontier show design trends and trade-offs between configurations that are more efficient in hover and those that are more efficient in high speed forward flight. The paper also introduces analytical insight into the effect known as lift offset which is an important design feature in coaxial configurations. This effect may be of advantage in terms of power consumption when configurations that consists of two main rotors (coaxial, tandem etc.) are operated at high speed forward flight.

1 Introduction

The notion *compound helicopter* stands for a vehicle that combines hover advantages of a helicopter and high speed flight capability by means of axial thrusters and fixed wings.

Classifications of early and present *compound helicopter configurations* are described

and discussed in Ref. 1,2. In such configurations, the auxiliary thruster system provides propulsive force in excess of the one provided by the rotors, while the wings provide lift in excess of the lift provided by the rotors, in particular at high forward flight speed. Usually, to maintain low rotor drag at high speed, it is necessary to slow down the rotor rotational speed to reduce compressible drag effects on the advancing blade. Thrusters may be implemented as either a “pusher” or as a “puller/tractor”. In this work, both cases will be referred to as a “pusher” without limiting the generality of the methodology.

In view of the above, compound helicopters attract tremendous interest in future full-scale and UAV-size as the demand for both VTOL and high speed capabilities seems to dominate all coming designs. Yet, the relevant literature shows that there are still major challenges in designing a compound configuration, where beyond high speed rotor system optimization, the most prominent issue is the determination of the optimal level of the pusher thrust as a function of speed and in particular, at what speed a pusher is essential. A related issue is the determination of the optimal wing sizing for a particular mission. On top of that, selecting an adequate analysis methodology for overall optimization of such configurations is still an open issue.

Detailed review of recent compound configurations may be found in Ref. 3

2 Analysis

To provide an insight into the problem under discussion, it is proposed to present it in wind axes directions, $\hat{x}_w, \hat{y}_w, \hat{z}_w$, see Fig. 1. As already in-

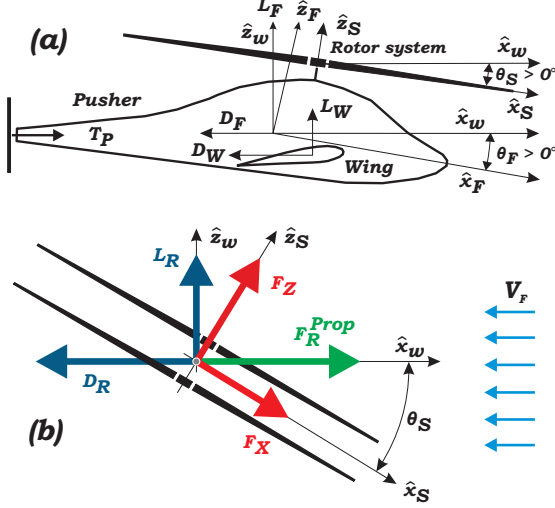


Fig. 1 Compound configuration in wind axes: (a) Side view; (b) Rotor loads.

dedicated, engaging a pusher and a wing is required mainly for achieving high speed forward flight, and therefore, the analysis will be focused on a specific forward flight speed, V_F , that constitutes a “high speed working point” for which a design is required.

As shown in Fig. 1, the fuselage axes are denoted $\hat{x}_F, \hat{y}_F, \hat{z}_F$, while the fuselage desired pitch attitude at V_F is denoted as θ_F . Regardless of any specific fuselage attitude, and for the sake of simplicity (without limiting the generality of the proposed analysis), it is assumed that the pusher is installed at an angle that will provide thrust in the \hat{x}_w direction, namely $T_P \hat{x}_w$. The fuselage drag and lift forces at the above attitude angle are denoted $-D_F \hat{x}_w$ and $L_F \hat{z}_w$, respectively. These values are extracted from suitable fuselage polars. Also shown in Fig. 1 are the rotor system’s shaft axes \hat{x}_S, \hat{y}_S and \hat{z}_S while the shaft axis (forward) tilt angle is denoted as θ_S . Note that for the sake of generality, θ_S is decoupled of θ_F (i.e. the rotor shaft mounting angle is not pre-assumed). Wing lift and drag are also shown in Fig. 1(a).

Rotor loads are shown in Fig. 1(b) where, for illustration purposes a coaxial system is pre-

sented. The rotor loads in the \hat{x}_S and \hat{z}_S directions are resolved into $F_R^{\text{Prop}} \hat{x}_w \equiv -D_R \hat{x}_w$ and $L_R \hat{z}_w$ where F_R^{Prop} , D_R and L_R are the rotor propulsive force, and the rotor drag and lift forces, respectively (all in wind axes). These are given by:

$$L_R = \sum_{m=1}^{N_R} \left[F_z^{(m)} \cos(\theta_S) - F_x^{(m)} \sin(\theta_S) \right], \quad (1)$$

$$D_R = \sum_{m=1}^{N_R} \left[-F_z^{(m)} \sin(\theta_S) - F_x^{(m)} \cos(\theta_S) \right] \quad (2)$$

where $N_R = 1$ or 2 for a single or a coaxial rotor, respectively, and $F_x^{(m)}$ and $F_z^{(m)}$ are each rotor forces in the shaft axes directions.

2.1 Drag vs. Power charts

To provide an insight into the problem, it is suggested to examine the “Drag vs. Power Chart” as shown in Fig. 2. This chart is drawn for the verti-

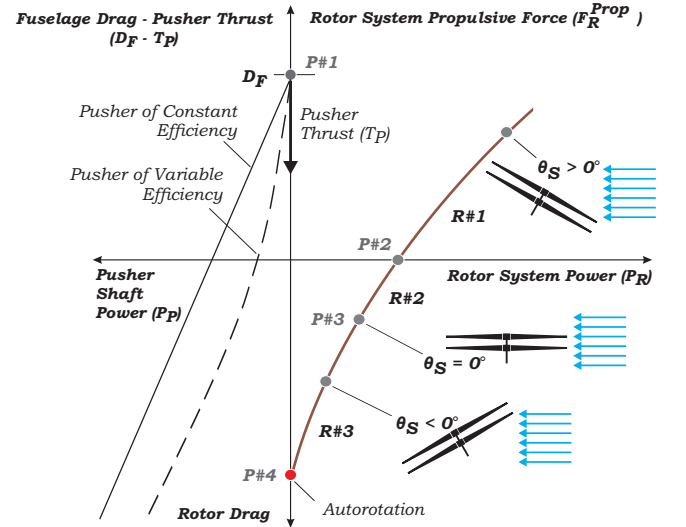


Fig. 2 Drag vs. Power chart: General description.

cal and longitudinal equilibrium of forces (other components will be dealt with later on) while assuming a constant speed (V_F), a given gross weight (GW) and a desired fuselage attitude (θ_F). Note that at this stage, there are no constraints on the selection of θ_F . For the sake of clarity, the wing will not be considered for the time being.

There are two types of curves in Fig. 2. We shall first discuss the rotor system DP line on

the right hand side. This line represents the rotor system “propulsive force” (or “drag” if it’s negative) as a function of its power consumption. This rotor line is drawn for constant L_R (the vertical force in the \hat{z}_w direction) while clearly: $L_R + L_F = GW$. This line is constructed by repeated analyses of the rotor system which differ only by their rotor shaft axis longitudinal attitude, θ_S , which is treated as a constant input for each analysis. These are “wind tunnel” type trim solutions and the way of executing such analyses is slightly different for a single rotor and a coaxial rotor system as explained in what follows.

For both single and coaxial rotor systems, at each point along the rotor DP line, the rotor shaft axis roll and heading angles are held at zero values. For a single rotor system, the calculations are focused on determining the 3 rotor controls $\theta_0, \theta_{1c}, \theta_{1s}$, that will satisfy the following 3 requirements:

$$L_R + L_F = GW, \quad (3)$$

$$\beta_{1c} = \beta_{1s} = 0, \quad (4)$$

where β_{1c} and β_{1s} are the first longitudinal and lateral flapping harmonic coefficients, respectively. Once a solution has been achieved, the corresponding rotor’s propulsive force, (F_R^{Prop}) and its power, P_R , are obtained and a point on the rotor DP line may be plotted.

For a coaxial system, the calculations are focused on determining the 6 rotor controls $\theta_0^{UR}, \theta_{1c}^{UR}, \theta_{1s}^{UR}, \theta_0^{LR}, \theta_{1c}^{LR}, \theta_{1s}^{LR}$ that will satisfy the following 6 requirements:

$$L_R + L_F = GW, \quad (5)$$

$$Q^{UR} = Q^{LR}, \quad (6)$$

$$\beta_{1c}^{UR} = \beta_{1s}^{UR} = \beta_{1c}^{LR} = \beta_{1s}^{LR} = 0, \quad (7)$$

where Q stands for the rotor torque. For introducing a lift-offset effect (see Ref. 4), one may replace the four equations of Eq. (7) by:

$$M_x^L = -M_x^U = \tilde{\epsilon}_L \frac{R}{2} \left(F_z^{(1)} + F_z^{(2)} \right) \quad (8)$$

$$M_y^L = M_y^U = 0, \quad (9)$$

where the nondimensional lift offset $\tilde{\epsilon}_L$ is defined as the differential roll moment divided by the total thrust and normalized by R .

Each point on this rotor DP line is characterized by the (local) rotor propulsive efficiency, η_R , given by

$$\frac{\partial F_R^{\text{Prop}}}{\partial P_R} = \frac{\eta_R}{V_F}.$$

Note that the above efficiency definition does not stand for “total propulsive force per total power required” (i.e. $F_R^{\text{Prop}} V_F / P_R$) at each point, but rather on the “change in propulsive force per unit change in required power” at each point.

For the examples presented in this paper, the above DP lines of the rotor were obtained using RAPID – Rotorcraft Analysis for Preliminary Design. RAPID is a desktop rotorcraft analysis software package. It is designed to model and analyze general rotorcraft and rotary-wing based configurations. All results presented in what follows were aerodynamically calculated with a free-wake model using a 2D lookup table technique for the blade cross-sectional aerodynamics. For the present purpose, rigid flapping blades were assumed. For more details see Ref. 5.

The lines on the l.h.s. of Fig. 2 are two typical pusher DP lines. Point P#1 indicates the fuselage drag (including the hub drag) (D_F) value discussed above. From that point and downwards, it is possible to draw the pusher thrust T_P . Hence, for any point below P#1 the vertical axis represents the value of $D_F - T_P$. For each level of pusher thrust (T_P), a value of pusher required power (P_P) may be determined and a point on this line may be drawn. For a pusher of constant efficiency, such a line is a straight one (since Fig. 2 is plotted for a constant speed). For a pusher of non-constant efficiency (where the pusher power is a nonlinear function of its thrust at the speed under discussion), such a line is generally curved. Similar to the rotor line, each point on this pusher DP line is characterized by the (local) pusher propulsive efficiency, η_P , given by

$$\frac{\partial T_P}{\partial P_P} = \frac{\eta_P}{V_F}.$$

For the sake of simplicity (and without limiting any of the generality of the proposed analysis), in this paper, straight pusher DP lines will

be dealt with (in which case the definition of the total pusher efficiency $T_P/P_P = \eta_P/V_F$ holds as well). The aerodynamic characteristics of the pusher propeller (such as diameter, number of blades and chord) are not dealt with here, as they are all embedded in its efficiency coefficient. Weight and location of the pusher propeller are not dealt with since longitudinal moment equilibrium is assumed to exist and as will be explained later on, the specific details of such equilibrium are decoupled from the main power issues discussed in the present paper.

Referring again to Fig. 2, clearly, in wind axes, longitudinal equilibrium requires that the rotor system propulsive force (F_R^{Prop}) will be equal to the “fuselage drag minus pusher thrust” ($D_F - T_P$). Therefore, the left and right hand sides of the vertical axis are labeled accordingly. Note again, that the above fuselage drag is based on the fuselage polars for the selected fuselage pitch (θ_F) at the present working point speed (V_F). For detailed description of Fig. 2, see Ref. 1.

2.2 Optimal Pusher Thrust level

Based on the above discussion, for any horizontal reference line that crosses the two DP lines in this chart, the rotor propulsive force, its power, the pusher thrust and its power are clearly obtained. These values may now be used for an insight into the problem of propulsive force and power sharing between the rotor system and the pusher.

In what follows, optimal pusher thrust for a given speed is defined as the value that minimizes the sum of the rotor system and pusher powers. The optimal pusher thrust is descriptively obtained by the contact point of the two DP lines when these are moved horizontally. A more precise determination of the minimum distance between these two curves shows that apart from points on the boundaries of these two DP lines, one should look for local minima values where

$$\frac{\partial F_R^{\text{Prop}}}{\partial P_R} = \frac{\partial T_P}{\partial P_P}. \quad (10)$$

Hence, at the optimal working point **any (small) amount of positive power shifted from the ro-**

tor to the pusher, will cause a reduction in the rotor propulsive force and increment in the pusher thrust of the same amount, and vice versa. Equation (10) may also be interpreted as equality of the (local) rotor and pusher propulsive efficiencies.

A typical DP chart is shown in Fig. 3 for a full scale configuration of $GW = 89\text{ kN}$ (20000 lb) with a coaxial rotor system at $V_F = 110\text{ m/s}$ ($\mu = 0.58$ for a tip speed of 190 m/s). The fuselage

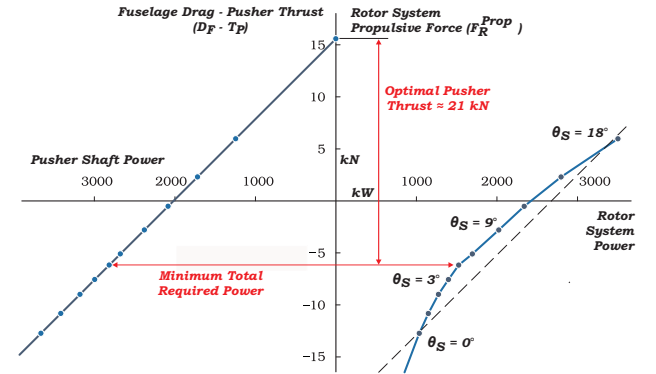


Fig. 3 Example of Drag vs. Power chart at $\mu = 0.58$ ($N_b = 4$ per rotor, $R = 8.18\text{ m}$, $\Omega = 23.23\text{ rad/s}$).

drag at that speed is about 15 kN . As shown by the rotor line of this chart, the rotor system provides propulsive force for θ_S above 12° and the rotor system autorotation is not achieved in the region explored. For that case, Fig. 3 clearly shows that the minimum total power is obtained for a pusher thrust of about 21 kN , and optimal configuration at that speed is obtained for a shaft tilt angle of about 4° .

Two important conclusions may be drawn here. First, pusher involvement may have an adverse effect, and secondly, at high speeds, trimming without a pusher is no longer possible. For example, as shown in Fig. 3, with a pusher thrust of less than $10 - 15\text{ kN}$, no trim may be achieved for practical shaft angles.

2.3 Adding a Wing to the DP Chart

As shown, the above DP chart treats separately the rotor system and the fuselage/pusher system. The later may be easily extended to a fuselage/pusher/wing system by shifting the pusher

power line upwards. The magnitude of this shift should be the amount of drag created by the wing at that speed. This may be determined as

$$D_W = \frac{L_W}{\left(\frac{L}{D}\right)_W}, \quad (11)$$

where L_W is the amount of lift carried by the wing and $\left(\frac{L}{D}\right)_W$ is the wing lift-to-drag ratio at V_F . In such a case, Eqs. (3) and (5) should be modify to

$$L_R + L_F + L_W = GW.$$

Note that for the sake of simplicity, a weight penalty due to the wing size is not included. Inclusion of such a penalty requires a relatively small augmentation of the gross weight. Figure 4 is drawn for a coaxial configuration and has

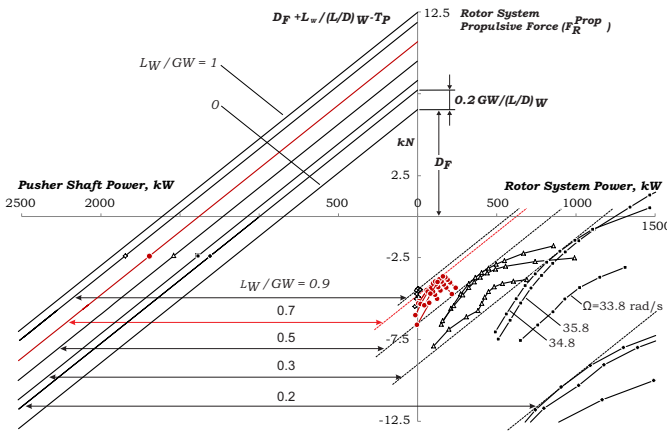


Fig. 4 Power consumption of a coaxial helicopter configuration with slowed rotor, a pusher and a wing at 110m/s ($N_b = 3$ per rotor, $R = 5.29\text{m}$, $\Omega = 23.8 \dots 35.88\text{rad/s}$).

two roles. The left hand side of it shows the pusher power required for a configuration with a wing that takes various levels of lift. These lines are drawn by Eq. (11) with vertical separation that corresponds to the wing lift level and for $\left(\frac{L}{D}\right)_W = 15$. Hence, any parallel line corresponds to a different value of L_W ($GW \geq L_W \geq 0$). As shown, as a fixed wing aircraft ($L_W = GW$), this configuration requires about 1600kW where a pusher thrust of about of 12.5kN is required.

The right hand side of this chart is also plotted for various L_W (by assuming that L_F is negligible and therefore $L_R = GW - L_W$) and for different rotational speed. As shown, minimum total power of about 2000kW is obtained for $L_W = 0.7GW$ with a pusher thrust of about 14.5kN (for $\Omega = 26.80\text{rad/s}$ and $\theta_s = 2^\circ$). This clearly demonstrates the penalty of having a rotor at relatively high forward flight speed compared with the “ideal” fixed wing aircraft at that speed. The substantial influence of the rotational speed is also evident. As shown, for such a configuration and speed, both pusher and a wing are essential as the power required for L_W which is lower than $0.3GW$ is not of practical magnitude.

2.4 Efficiency of Compound Helicopter vs. Fixed Wing

In order to compare the efficiency of a compound-helicopter (CH) and a fixed-wing (FW), we define the “total compound configuration efficiency” as the ratio between the net (minimum) power required (due to the fuselage drag only) to the total power consumed, namely:

$$\eta_{CH} = \frac{D_F V_F}{P_R + P_P}.$$

Along the same lines, “fixed wing efficiency”, for the case where a wing supplies lift and the pusher supplies propulsive force (and no rotor exists) may be defined (for the case of a pusher with linear T_P vs. P_P dependency) using $T_P/P_P = \eta_P/V_F$ as:

$$\eta_{FW} = \frac{D_F V_F}{\left[D_F + \frac{GW}{\left(\frac{L}{D}\right)_W} \right] \frac{V_F}{\eta_P}} = \eta_P \frac{\left(\frac{L}{D}\right)_W}{\left(\frac{L}{D}\right)_W + \frac{GW}{D_F}},$$

which for the typical values of $\eta_P \approx 0.85$, $\left(\frac{L}{D}\right)_W \approx 15$ and $\frac{GW}{D_F} \approx 9$ yields a relatively high value of $\eta_{FW} \approx 0.53$.

3 Trade-offs Optimization and Design Trends

The problem of minimizing the total power required for a compound helicopter has been tradi-

tionally handled by standard optimization tools. These may vary between simple modifications of design variables for minima search (“parametric study”) up to a formal optimization of a cost function over the entire range of the design variables. In this paper, we demonstrate two different levels of optimization. First, a “global search” level is presented. Then, two versions of a “local search” level are offered. All versions in this local search level are based on initial configurations obtained by the global search. Local search is based on “random local search” or “derivatives-based local optimization” procedures as will be clarified later on.

Similar to the previously discussed numerical analyses, in this section we shall present results of detailed trim cases in hover and forward flight that were obtained by RAPID. These are 6DOF analyses where rotor aerodynamics is determined by a free-wake model and a 2D lookup table technique. Fuselage aerodynamics is based on experimental polars.

Since optimizing a configuration is required over a wide range of speeds, an optimization method that accounts for trade-offs between hover and various forward flight speeds is essential. For that purpose, Pareto Frontier (see e.g. Ref. 6) based methodology was adopted. Hence, to build a 2D Pareto frontier, one may set two different criteria by which each feasible configuration should be compared with other configurations. In this paper, these criteria were selected to be the hover power required and the forward flight power required. To cover a wide range of forward flight speeds, we have created a 2D Pareto frontier for selective forward flight speeds (while each of them is matched against hover) as will be shown in what follows. The analysis was therefore focused on hover and cruise speeds of 30, 50, 70, 90, 110 m/sec ($\simeq 58$ to 213 kts). In this context, the notion “configuration” stands for a predetermined set of coaxial/single rotor system with/without a wing with/without a pusher. Within this set, the optimization is searching for the best set of “design parameters” while all other are considered constants.

It should be indicated again, that each point along the Pareto frontier stands for a configura-

tion. Hence, studying the changes of particular characteristics along the frontier shows the design changes (i.e. trends) required to achieve the power trade-offs between configurations that are better for hover and those that are better for forward flight (while all configurations can be operated in both regimes).

3.1 Global Search

For initial demonstration of the optimization process, we have selected a configuration of a pusher powered coaxial system with a wing. All configurations involved were of a gross weight of 9000 kg ($\simeq 20,000 lb$) and operated at sea level.

At this stage it is important to note that the trim requirement for a configuration to become feasible may be too restrictive. In many cases, trim was not achieved due to non-trimable pitching moment that is a result of unsuitable wing or rotor hub location relative to the center of gravity, and small modifications in these parameters could allow trimming. This issue stresses again the advantages of preliminary analysis using the DP chart methodology presented earlier that does not account for the configuration pitching moment while the pusher thrust is not randomly selected but obtained as the value that minimizes total power.

To draw the Pareto frontier we have eliminated all points that are dominated by other points. To further explain, we shall define $H(I)$ as the hover power of design “I” and $F(I)$ as the forward flight power of it. Then, by looking at two designs “A” and “B”, one may define $\Delta_H = H(B) - H(A)$ and $\Delta_F = F(B) - F(A)$. Subsequently, design “A” dominates design “B” if $\Delta_H \geq 0$ and $\Delta_F \geq 0$. In a rare cases where $\Delta_H = \Delta_F = 0$, these two designs are equivalent in terms of power consumption in both hover and the forward flight speed under discussion, and one should select a dominant design based on other criteria.

Figure 5 shows the corresponding Pareto frontier for $V_F = 30, 50, 70, 90, 110 m/s$ in addition to all feasible configurations that were created in this process. As shown, there is a clear trade-off between hover and forward flight power

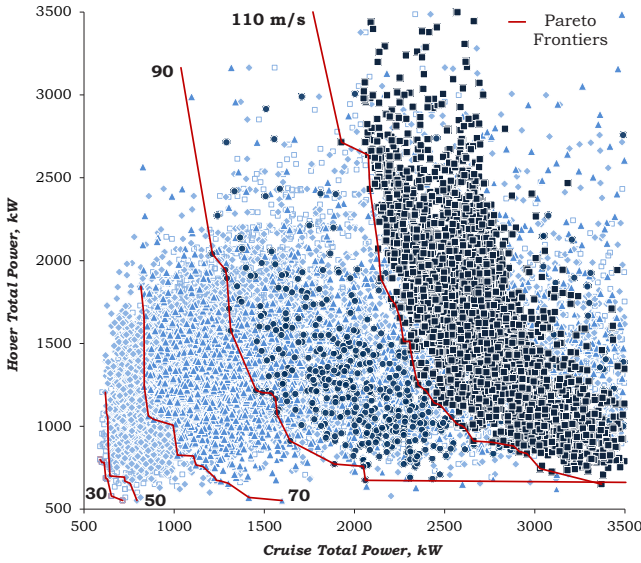


Fig. 5 Pareto frontiers for $V_F = 30, 50, 70, 90, 110\text{m/s}$.

consumption. For example, at $V_F = 70\text{m/s}$, a configuration that requires about 1000kW for both hover and forward flight is feasible. However, reducing the hover power to 600kW will cost about 1400kW in forward flight, and any reduction in forward flight power will cause a substantial increase in hover power. This trend is similar for higher speeds while hover power increase is less sharp. Hence, hover-cruise trade-offs are more limited at relatively low speed cases.

3.2 Local Search and Optimization

To refine the Pareto frontier that has been obtained by global search one may apply a search for local minima (if they exist) over the entire Pareto frontier or only over areas of interest along it.

Random local search is similar to the global one but is based on random selection of configuration in a smaller range around some initial configuration. When such a technique is employed, almost all trial configurations converge for trim. Hence, improved frontier may be obtained when the initial configuration is one that was located on the Pareto frontier as obtained by the global search.

In addition, derivatives based local search

may be applied. Fig. 6, shows derivatives with

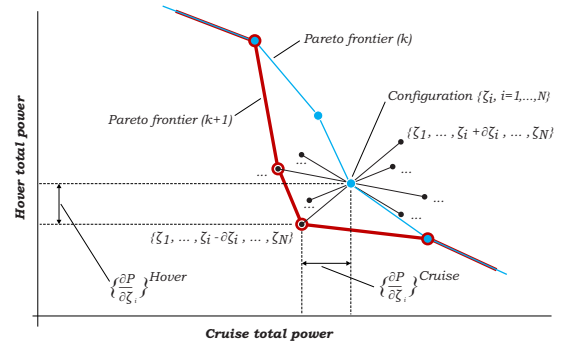


Fig. 6 Influence of small design changes about a point on the Pareto frontier.

respect to various design parameters. Each finite (small) change in a design parameter ζ_i (such as radius, pusher thrust, average chord, chord taper, twist, rotational speed, etc.) results in a change in both hover and forward flight power. These may be plotted as two points (that stand for positive and negative perturbations) at the end of line segments that passes through the initial point (these are almost straight lines since the changes are small).

All points obtained by the one or more versions of the local search may be considered now as new candidates for the frontier, and they will replace all existing points on the frontier that they dominate.

When the above technique is applied and a new frontier is obtained, the process may be repeated for all or some of the points on the new frontier. Such an update of the frontier creates an improved frontier at each stage. As already indicated, this technique may also be directed towards region of interest on the frontier if design of a configuration in that region of power consumptions (in hover and forward flight) is required.

3.3 Design Trends

Design trend of the pusher thrust is shown in Fig. 7. As shown, for a configuration that is better in forward flight, less pusher thrust is required. Design trend of the required lift offset is shown in Fig. 8. clearly, lift offset reduces the required

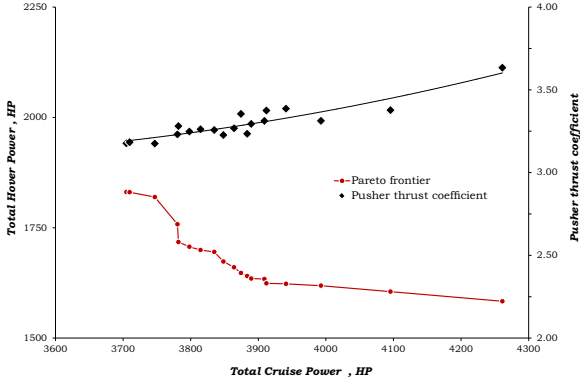


Fig. 7 Design trend of the pusher thrust (cruise speed = 113.2 m/s = 220 knots).

power in coaxial configuration at high speed.

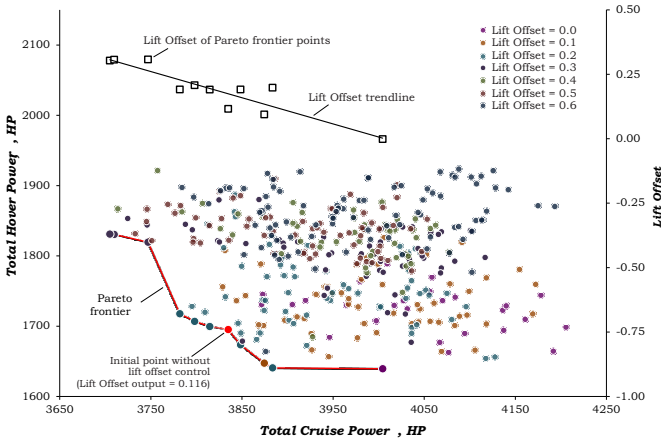


Fig. 8 Design trend of the required lift offset (cruise speed = 113.2 m/s = 220 knots).

4 Analytical Modeling of the Lift offset effect

Operating a rotor with non-zero lift offset is achieved by creating a non-zero roll moment while keeping zero pitch moment. Lift offset is fundamentally created by a larger lift on the advancing blade relative to the retreating blade lift. Hence, when a non-negligible roll moment is involved, such operation is practical only in configurations that consist of two main rotors (coaxial, tandem etc.) where each rotor creates an equal and opposite roll moment. Generally speaking, in such configurations, the roll moments are affected by the mutual interaction between the rotors and therefore, different controls are required

to achieve a balanced system. Yet, the phenomena associated with the power consumption in the presence of lift offset may also be studied for one of the rotors that produces roll moment with no interaction effects. For more details and related discussion - see Refs.4,7-9.

In a rotor system that consists of two rotors, lift offset is defined as the differential moment divided by the total thrust of the system and the rotor radius. To supply an insight into the mechanism, we examine a rotor in edgewise flight where the nondimensional lift offset should be defined as

$$\tilde{e}_L = \frac{C_{M_x}}{C_T}, \quad (12)$$

where C_{M_x} and C_T are the roll moment and thrust coefficients, respectively.

Hence, strictly speaking, the above definition is valid for a coaxial system when the interaction between the rotors is not accounted for. In a case of coaxial rotor system (or for two tandem rotors that are closely spaced) that are operated in hover or low speed forward flight, the thrust on both rotor may be different but roll moment trim will still require equal (and of opposite sign) roll moments of both rotors. However, lift offset in hover and low speed is not of interest in the present context of using lift offset to extend the flight envelop for high speed edgewise flight in terms of power consumption.

Consider a rotor of radius R and N_b blades of constant chord c in edgewise forward flight, V_F . The rotor rotates at a constant angular velocity, Ω , and the disk is tilted forward at α_D .

To demonstrate the lift offset effect, we assume that the lift coefficient radial and azimuthal distribution is of the form

$$c_l(\tilde{r}, \psi) = c_l^0 \tilde{r}^n (1 + A_s \sin \psi), \quad (13)$$

where c_l^0 is the average value of the blade tip lift coefficient and A_s serves as its sine amplitude. Both c_l^0 and A_s are independent of \tilde{r} and ψ and will be determined by the $\frac{C_T}{\sigma}$ and \tilde{e}_L of the case under discussion. The power of the radial variation, n , is an assumed parameter (not necessarily an integer) that describes the lift coefficient radial distribution while analytical considerations

shown later on require $n > \frac{1}{2}$. As a reference, it should be noted that in hover, $n = 1$ corresponds to a linear lift distribution along the blade (i.e., ideal constant thrust per unit disk area and uniform inflow).

With the sectional free stream velocity

$$\tilde{U} = \tilde{r} + \mu \sin \psi, \quad (14)$$

the nondimensional lift per unit blade length takes the form

$$\frac{\partial L / \partial r}{\rho \Omega^2 R^3} = \frac{1}{2} \tilde{U}^2 \tilde{c}_l. \quad (15)$$

The above definitions enable to express and analytically evaluate the thrust coefficient as

$$C_T = \sigma c_l^0 \left[\frac{1}{2(n+3)} + \mu \frac{A_s}{2(n+2)} + \mu^2 \frac{1}{4(n+1)} \right], \quad (16)$$

from which c_l^0 is extracted as a function of $\frac{C_T}{\sigma}$ and may be written as

$$c_l^0 = \frac{C_T}{\sigma} \frac{1}{\left[\frac{1}{2(n+3)} + \mu \frac{A_s}{2(n+2)} + \mu^2 \frac{1}{4(n+1)} \right]}. \quad (17)$$

Roll (left) and pitch (up) moments are then determined and analytically evaluated as $C_{M_y} = 0$ and

$$C_{M_x} = \sigma c_l^0 \left[\frac{A_s}{4(n+4)} + \mu \frac{1}{2(n+3)} + \mu^2 \frac{3A_s}{16(n+2)} \right]. \quad (18)$$

Hence, the lift offset defined by Eq.(12) is directly extracted from Eqs. (16),(18) as

$$\tilde{e}_L = \frac{\frac{A_s}{4(n+4)} + \mu \frac{1}{2(n+3)} + \mu^2 \frac{3A_s}{16(n+2)}}{\frac{1}{2(n+3)} + \mu \frac{A_s}{2(n+2)} + \mu^2 \frac{1}{4(n+1)}}, \quad (19)$$

from which the lift coefficient sine amplitude is obtained as

$$A_s = \frac{\frac{\tilde{e}_L}{2(n+3)} - \mu \frac{1}{2(n+3)} + \mu^2 \frac{\tilde{e}_L}{4(n+1)}}{\frac{1}{4(n+4)} - \mu \frac{\tilde{e}_L}{2(n+2)} + \mu^2 \frac{3}{16(n+2)}}. \quad (20)$$

As expected, introducing lift offset in hover increases the lift coefficient variation over the disk. For example, for $n = 1$ (linear lift radial distribution that corresponds to ideal constant thrust

per unit disk area and uniform inflow), one obtains

$$c_l = 8 \frac{C_T}{\sigma} \tilde{r} \left(1 + \frac{5}{2} \tilde{e}_L \sin \psi \right), \quad (21)$$

which is bound to increase power consumption as will be discussed later on. Similar behavior is obtained for very low advance ratios.

A measure of the azimuthal variation of the lift coefficient may be easily defined since c_l maximum and minimum values are always observed at $\psi = \pm \pi/2$. One may therefore define the maximal difference in c_l at the blade tip as $\Delta c_l = c_l(\tilde{r} = 1, \psi = -\frac{\pi}{2}) - c_l(\tilde{r} = 1, \psi = \frac{\pi}{2})$ which according to Eq.(13) becomes

$$\Delta c_l = -2c_l^0 A_s. \quad (22)$$

Figure 9 shows the blade tip lift coefficient

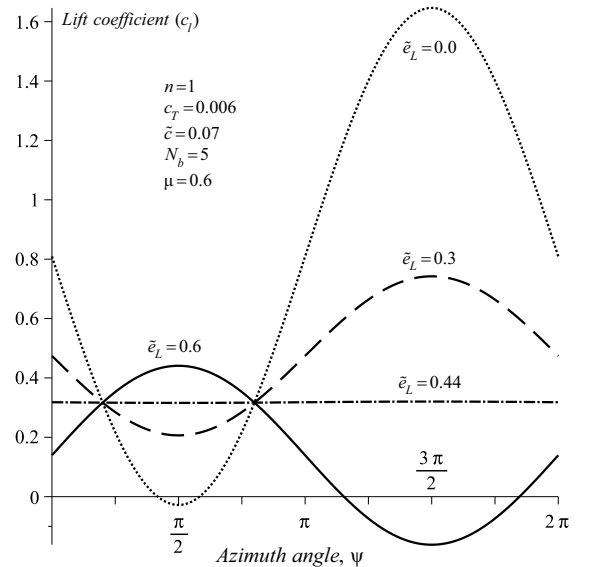


Fig. 9 Tip cross-section lift coefficient vs. azimuth angle for various lift offset values.

distribution as function of the azimuth angle for four values of lift offset values. As shown, operating a rotor with nonzero lift offset requires much lower lift coefficients. For a specific lift offset value the lift coefficient is constant and constitutes the minimal (positive) value required. Even for the case shown in Fig.(9), operating with zero lift offset is questionable due to the relatively high lift coefficients required, but it is definitely possible to double the disk loading if lift

offset is introduced. This characteristic of the lift offset will be proved in what follows to have a major contributions to the lower values of power required.

Figures 10 provides correlation of the present

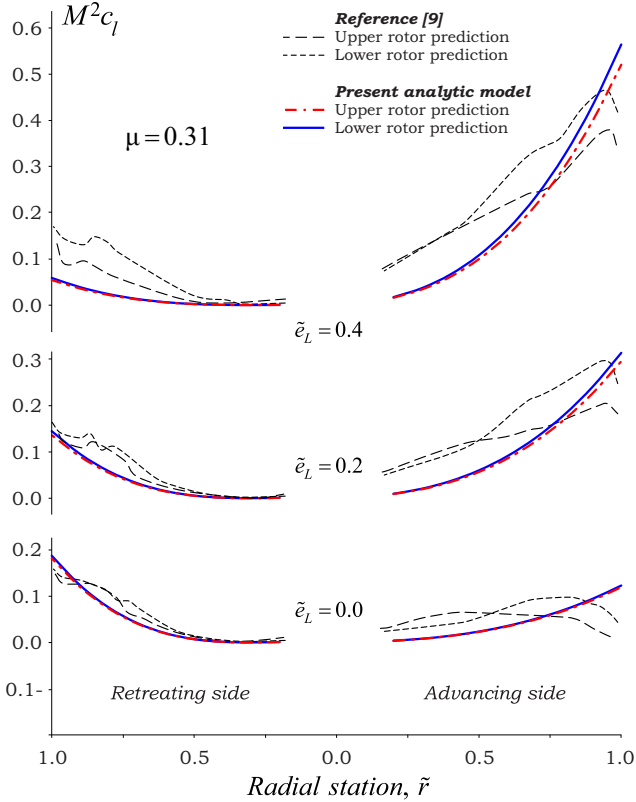


Fig. 10 Cross-sectional lift vs. radial station, correlation with Ref.9 for $\mu = 0.31$ ($n = 1$).

method results with those that were generated by a detailed comprehensive numerical modeling presented by Yeo and Johnson in Ref.9 for $\mu = 0.31$. As shown, the present model provides a very good approximation to the actual lift distribution. It well provides differential lift on the advancing and retreating sides that fundamentally creates the lift offset. Note that the slightly different lift distributions over the upper and lower rotors are due to the small differences in the thrust coefficients obtained in Ref.9. Hence, Figs. 10 serves also as demonstrators to the fact that the phenomena associated with lift offset in coaxial configurations are primarily associated with the lift distribution over each one of the rotors and that the interactional effects should be considered

as minor in view of the present attempt to analytically explain the associated phenomena.

5 Conclusion

This paper presents a study of design and optimization aspects of compound helicopter configurations with an emphasis on the role of an axial thruster and a wing in addition of design trends. A Drag vs. Power (DP) chart is proposed for the examination of the associated characteristics of the rotor system, the fuselage, the thruster and the wing. Such a point of view results in important insights into various aspects of the problem and became instrumental during the global optimization process as well. DP charts demonstrate the trade-offs in this extremely involved and complex optimization problem and are applicable for both single and coaxial rotor systems.

DP charts clearly show that for a given forward speed, the optimal pusher thrust level is a function of both the propulsive efficiency of the rotor system and the propulsive efficiency of the pusher. In the general case, both efficiencies are nonlinear functions (in the present context, the rotor system efficiency is a nonlinear function of its propulsive force for a given lift and the pusher efficiency is a nonlinear function of its thrust level - both at a given forward flight velocity).

The present effort also offers a generic and fully nonlinear optimization process. In this process, initial collection of configurations is constructed by randomly selection of the design variables. Then, a Pareto frontier is assembled for various forward flight speeds power vs. hover power. While all configurations on the Pareto Frontier are feasible for both hover and forward flight, examination of the configurations along the frontier yields the required design trade-offs between configurations that are more efficient in hover and those that are more efficient in forward flight.

It was shown that the rotor DP line as a function of its parameters and in particular its lift level, flight velocity, tilt angle and rotational speed, is the most important data required for preliminary optimization of the whole system.

Such data should be provided by suitable analysis schemes. Since various nonlinear behavior of such DP lines were examined in this study, it is reasonable to conclude that the overall insight provided will be valid over a wide range of configurations.

Overall, by providing insight into the problem, the methodology presented in this paper is capable of challenging some common intuitive design trends for compound helicopter configurations.

References

- [1] Rand, O., Khromov, "Compound Helicopter: Insight and Optimization," *American Helicopter Society 69th Annual Forum, Phoenix, Arizona, May 21–23, 2013*.
- [2] Robb, R. L., "Hybrid Helicopters: Compounding the Quest for Speed," *Vertiflite*, Vol. 52,(2), Summer 2006.
- [3] Hirschberg, M., "X2, X³, S-97 and X-49: The Battle of the Compounds is Joined," *Vertiflite*, Vol. 56, (4), Winter 2010.
- [4] Johnson, W., "Influence of Lift Offset on Rotorcraft Performance," American Helicopter Society Specialist's Conference on Aeromechanics Proceedings, San Francisco, CA, January 23-25, 2008.
- [5] Rand, O., "RAPiD - Rotorcraft Analysis for Preliminary Design, User Guide 2012," TAE 987 Report, Technion - Israel Institute of Technology, Faculty of Aerospace Engineering, Haifa, Israel, July 2012.
- [6] Steuer, R.E. *Multiple Criteria Optimization: Theory, Computations, and Application*, New York: John Wiley & Sons, Inc., 1986.
- [7] Johnson, W., Yamauchi G.K, and Watts, M.E., "NASA Heavy Lift Rotorcraft Systems Investigation," NASA/ TP-2005-213467, December 2005.
- [8] Johnson, W., Moodie, A.M, and Yeo, H., "Design and Performance of Lift-Offset Rotorcraft for Short-Haul Missions," Proceeding of 2012 AHS Future Vertical Lift Aircraft Design Conference, San Francisco,CA, January 18-20, 2012.
- [9] Yeo, H., and Johnson, W., "Investigation of Maximum Blade Loading Capability of Lift-Offset Rotors," Proceeding of 2013 AHS 69th Annual Forum, Phoenix, Arizona, May 21-23, 2013.

6 Contact Author Email Address

Omri Rand: omri@sni.technion.ac.il

Vladimir Khromov: rapid@technion.ac.il

Copyright Statement

The authors confirm that they, and/or their company or organization, hold copyright on all of the original material included in this paper. The authors also confirm that they have obtained permission, from the copyright holder of any third party material included in this paper, to publish it as part of their paper. The authors confirm that they give permission, or have obtained permission from the copyright holder of this paper, for the publication and distribution of this paper as part of the ICAS 2014 proceedings or as individual off-prints from the proceedings.